Supplement of Atmos. Chem. Phys., 26, 3001–3024, 2026
https://doi.org/10.5194/acp-26-3001-2026-supplement

Atmospheric Chemistry and Physics
Open Access
EGU

Supplement of

Distinct spatiotemporal patterns of atmospheric total and soluble iron from three sources revealed by shipboard online observations in the Northwest Pacific

Tianle Zhang et al.

Correspondence to: Mei Zheng (mzheng@pku.edu.cn)

S1. Comparison of atmospheric Fe concentrations between online Xact 625 and offline filter analysis during the BY cruise

The comparison of atmospheric Fe concentrations measured by the online Xact 625 instrument and offline filter-based inductively coupled plasma mass spectrometry (ICP-MS) analysis is shown in Fig. S2. After excluding one outlier (sample BY9), the remaining samples exhibit comparable concentrations, with an R^2 of 0.80 and a slope of 0.85.

The only sample that exhibited a poor comparison between the online and offline Fe detection methods (Fig. S2) was the BY9 sample, which was collected during an intense dust event (Section 3.1.2 in the main text). Consequently, coarse particles experienced significant losses due to inertial impaction in the sampling tubing of Xact 625, resulting in substantially lower concentrations of dust-related elements in PM_{10} measured by the online Xact 625 compared with offline filter-based analyses, such as Fe (online: 762.4 ng m^{-3}; offline: 1680 ng m^{-3}) and Ca (online: 1119 ng m^{-3}; offline: 1938 ng m^{-3}). In contrast, fine-mode anthropogenic elements showed no such discrepancy, such as Pb (online: 7.88 ng m^{-3}; offline: 6.18 ng m^{-3}) and Cu (online: 3.54 ng m^{-3}; offline: 3.57 ng m^{-3}).

This underestimation mainly affects crustal elements rather than fine-mode elements and would therefore lead to an underestimation of the dust contribution in the PMF analysis based on online data. However, the PMF results already indicate an overwhelming dust contribution of 96% during the BY9 sampling period, supporting our conclusion that Fe during this sampling period was dominated by dust source. Therefore, the underestimation introduced by particle losses is considered minor and will not affect the main conclusions.

Besides, we note that the online–offline comparison during the BY cruise was affected by specific sampling conditions. During the BY cruise, the Xact 625 instrument was installed inside the main deck laboratory, connected to the sampling inlet via a relatively long (~10 m) sampling tubing, which might result in sampling loss of large particles. In contrast, during the NWP1 and NWP2 cruises, the instrument was installed in a foredeck container and connected to the sampling inlet using a short, vertically oriented sampling tubing of approximately 1 m, which likely minimized particle losses.

S2. Analytic procedure for filter samples

For total elements digestion, an entire PTFE filter (46.2 mm diameter, Whatman) was cut into fragments and placed in a PTFE digestion jar. Prior to use, all digestion jars were rigorously cleaned with deionized water, hydrochloric acid (HCl), and nitric acid (HNO_3), following the procedure described in Zhang et al. (2022). The filter fragments were first pre-digested at room temperature for 12 hours with 2 mL of HNO_3 (69% w/w) and 2.5 mL of hydrogen peroxide (H_2O_2) (31% w/w), followed by the addition of 3 mL HNO_3 (69% w/w) and 1 mL hydrofluoric acid (HF) for microwave digestion. Digestion was carried out using a microwave digestion system (TOPEX+, PreeKem Co., Ltd.) under a temperature-controlled program: ramp to 50 °C in 5 min and hold for 5 min; ramp to 120 °C in 10 min and hold for 15 min; ramp to 180 °C in 10 min and

hold for 30 min; followed by a 20 min cooling phase to 50 °C. After digestion, the jars were transferred to a heating plate and heated at 140 °C to evaporate residual acids to near-dryness. The digestates were then reconstituted to 20 mL with 1% (v/v) HNO_3 and filtered through a 0.22 μm pore-size polyethersulfone (PES) syringe filter.

For soluble element extraction, another entire PTFE filter (46.2 mm diameter, Whatman) was cut into fragments and placed in a centrifuge tube. A 5 mM ammonium acetate-acetic acid buffer solution (pH 4.7) was freshly prepared by dissolving 0.7758 g ammonium acetate and 571 μL acetic acid in 2 L ultrapure water. Each centrifuge tube containing filter fragments was treated with 10 mL of the buffer solution, sealed tightly, and horizontally shaken (ZWHZ-08A oscillator, 300 rpm) for 2 hours at room temperature. After shaking, the supernatant was filtered through a 0.22 μm PES syringe filter and collected into pre-labeled centrifuge tubes. Subsequently, 144 μL of HNO_3 (69% w/w) was added to each tube to obtain a final test solution with a substrate of 1% (v/v) HNO_3.

Elemental concentrations of Al, Fe, Ba, Mn, Cr, Cu, Zn, Pb, V, Ni, As, Se, Cd, and Sb were quantified using inductively coupled plasma mass spectrometry (ICP-MS; iCAP Q, Thermo Fisher Scientific). Four field blanks were analyzed, including two for acid digestion and two for buffer extraction. Elemental concentrations in ambient samples were corrected by subtracting the blank value.

S3. Definition and screening method for outliers

Outlier screening was conducted in two steps: automated screening followed by manual verification. The automated screening was performed using custom MATLAB code. In the script, a variable called the "beside-mean" was defined. For instance, the beside-mean of Fe in the 100th sample was calculated as the average concentration of Fe in the 98th, 99th, 101st, and 102nd samples. If the Fe concentration in the 100th sample exceeded 1.8 times or was less than 0.2 times its beside-mean (>1.8×beside-mean or <0.2×beside-mean), it was automatically flagged as an outlier.

The flagged outliers were then subjected to manual review. An outlier was confirmed manually only if it met both of the following criteria: (1) the outlier was temporally discontinuous, with no abnormal concentrations observed in the adjacent samples; and (2) only one element associated with a specific source showed an abnormal concentration in the sample, while other elements associated with the source in this sample remained within normal ranges.

S4. Preparation of input data for Positive Matrix Factorization (PMF)

Positive Matrix Factorization requires the input of both measured chemical species concentrations and their associated uncertainties. For concentration data, values below the minimum detection limit (MDL) were replaced with half the MDL.

For uncertainty calculations, two approaches were applied based on the measured concentration relative to the MDL. If the concentration of a species was less than or equal to the MDL, the uncertainty (Unc) was calculated as a fixed fraction of the MDL, as shown in Equation (S1). If the concentration exceeded the MDL, the uncertainty was calculated using Equation (S2), where the error fraction was set to 0.2.

$$\text{Unc} = \frac{5}{6} MDL \quad \text{(S1)}$$

$$\text{Unc} = \sqrt{(Error\ Fraction \times concentration)^2 + (0.5 \times MDL)^2} \quad \text{(S2)}$$

S5. Testing of the PMF model

The number of factors in the PMF model was selected using two criteria: (1) diagnostic indicators recommended in the EPA PMF 5.0 User Guide (Gary et al., 2014), and (2) the allocation of source tracers within each factor. Using the PM_{10} samples source apportionment as an example, the number of factors was varied from three to eight to identify the optimal solution. As shown in Equation (2) in the main text, the objective function Q is an important parameter of the PMF model, which produces two types of Q values: Q_{true} (the goodness-of-fit parameter calculated using all points) and Q_{robust} (the goodness-of-fit parameter calculated excluding points not fit by the model, defined as samples with uncertainty-scaled residuals greater than 4). In this study, as the number of factors increased, the ratio of Q_{true} to Q_{robust} remained between 1.2 and 1.6, which indicated limited influence from data points with large residuals. Meanwhile, the value of Q_{robust} relative to $Q_{expected}$ (as calculated in Equation (S3)) reached its minimum at seven factors, which suggested that the mathematical diagnostics favored a seven-factor solution, as it produced the lowest residuals.

$$Q_{expected} = n \times m - p \times (n + m) \quad \text{(S3)}$$

Where n is the number of chemical species (only those marked as strong in the model are included), m is the sample size, p is the number of factors.

Despite this, closer examination of the seven-factor profiles revealed several factors that were difficult to interpret. Some factors were dominated solely by Se, Ni, or Ca, without other supporting tracers, making it difficult to link them to specific emission sources. In contrast, reducing the model to three factors eliminated these anomalous single-element factors, and each factor exhibited a clear association with an identifiable source. Furthermore, a detailed comparison of the 3–5 factor solutions is provided in Table S1. According to Table S1, in the three-factor solution, the three factors correspond to dust, ship emission, and land-based anthropogenic sources, respectively. When transitioning from a three-factor to a four-factor solution, a factor characterized by only Ca emerged. While Ca may originate from sea salt in addition to dust source, this factor shows only a weak correlation with wind speed (correlation coefficient of 0.11), making it unlikely to represent a sea spray source. Additionally, when moving from the four-factor to the five-factor solution, the land anthropogenic source factor appeared to split into two factors, neither of which could be clearly attributed to a specific source. Therefore, the three-factor solution was selected, as it identified distinct and interpretable sources.

Under the three-factor solution, Fe concentrations were reconstructed from the PMF outputs according to Equation (S4). The reconstructed Fe concentrations correlated strongly with the measurements, with R^2 equal to 0.88 and a linear regression slope of 1.14 as shown in Fig. S4a. This result indicated that the three-factor solution provided strong predictive capability for ambient Fe concentrations.

$$\mathrm{PMF\_Fe_i} = \sum_{j=1}^{3}(Fe_j \times R_{i,j}) \quad \text{(S4)}$$

Where $\mathrm{PMF\_Fe_i}$ represents the PMF-reconstructed Fe concentration in sample i (unit: ng m^{-3}); $\mathrm{Fe_j}$ denotes the Fe concentration in the profile of factor j (unit: ng m^{-3}); $\mathrm{R_{ij}}$ indicates the contribution of the factor j to sample i (dimensionless).

We applied the same source analysis approach to Fe in $PM_{2.5}$ samples from the NWP1 cruise. Testing different factor numbers again identified a three-factor solution as optimal. As shown in Table S2, the characteristic elements of each factor in the 3-5 factor solutions again highlighted dust, ship, and land anthropogenic sources form the most interpretable combination of factors. The reconstructed Fe concentrations agreed well with the measured values, with R^2 equal to 0.85 and a linear regression slope of 1.21 as shown in Fig. S4b.

Table S1. Characteristic elements in each factor from PMF analysis of PM_{10} samples

	Three-factor solution	Four-factor solution	Five-factor solution
Factor 1	Ca, Ba, Fe, V, Mn [a] Dust source [b], 59.3% [c]	Ba, Ca, Fe, V, Mn Dust source, 56.0%	Ba, Ca, Fe, V, Mn Dust source, 54.5%
Factor 2	Ni, V Ship emission, 5.7%	Ni, V Ship emission, 3.7%	Ni, V Ship emission, 3.2%
Factor 3	As, Pb, Zn, Se, Cu, Mn, Ba, Fe Land anthropogenic sources, 35.0%	As, Zn, Pb, Se, Cu, Mn, Fe, Ba Land anthropogenic sources, 38.5%	As, Se, Zn, Mn Coal burning? Industry? 28.1%
Factor 4		Ca ?, 1.8%	Ca ?, 0.9%
Factor 5			Pb, Cu, Ba Industry? Brake and tire wear? 13.4%

[a] Characteristic elements in a factor are defined as those where the factor's contribution to the element exceeds 30%, and the elements are sorted by factor contribution;
[b] Emission sources are named according to the factor profiles, with "?" indicating sources that are difficult to identify;
[c] The value represents the contribution of the factor to the target element Fe.

Table S2. Characteristic elements in each factor from PMF analysis of $PM_{2.5}$ samples

	Three-factor solution	Four-factor solution	Five-factor solution
Factor 1	Ca, Ba, K, Fe, Cu, Mn [a] Dust source [b], 59.8% [c]	Ba, Fe, Ca, Mn, K Dust source, 64.1%	Ba, Fe, Ca, Mn Dust source, 57.0%
Factor 2	V, Ni Ship emission, 3.5%	V, Ni Ship emission, 2.2%	V, Ni Ship emission, 0.8%
Factor 3	As, Zn, Se, Pb, Mn, Fe Land anthropogenic source, 36.7%	As, Zn, Se, Pb, Mn Land anthropogenic source, 22.5%	Se, As, Pb Coal burning? Industry?, 13.7%
Factor 4		Cu, K, Ca ?, 11.2%	Ca, K, Cu ?, 12.3%
Factor 5			Zn, Pb, Mn, Cu Industry? Coal burning?, 16.2%

[a] Characteristic elements in a factor are defined as those where the factor's contribution to the element exceeds 30%, and the elements are sorted by factor contribution;
[b] Emission sources are named according to the factor profiles, with "?" indicating sources that are difficult to identify;
[c] The value represents the contribution of the factor to the target element Fe.

Table S3. Elemental concentration in marine aerosols over the Chinese marginal Seas and the open Northwest Pacific based on measurements (unit: ng m^{-3})

	This study			Shimada et al. (2018)		Ge et al. (2024)	Zhang et al. (2024)		Jin et al. (2019)
Sea area	BY cruise	NWP1 cruise	NWP2 cruise	Tuoji Island, Bohai Sea	Cape Hedo, East China Sea	Chinese marginal Seas	Yellow Sea and East China Sea	Open Northwest Pacific	Open Northwest Pacific
Time	April, 2022	May-June, 2021	June-July, 2022	2012-2014		November, 2021	March-May, 2015		March-April, 2016
Size	PM_{10}	$PM_{2.5}$	PM_{10}	$PM_{2.5}$	$PM_{2.5}$	TSP[#]	$PM_{2.5}$	$PM_{2.5}$	TSP
K	2305 ± 730.0*	84.80 ± 51.00	475.0 ± 169.8	287.0 ± 48.0	91.9 ± 8.85	/	369.2 ± 225.9	149.5 ± 77.60	97.8~386.1
Ca	247.1 ± 362.3	47.00 ± 34.60	106.5 ± 105.3	605.7 ± 51.2	65.8 ± 7.26	/	139.9 ± 139.3	126.6 ± 117.9	/
Fe	228.5 ±281.5	54.90 ± 52.48	35.56 ± 99.94	194.0 ± 27.3	51.3 ± 6.73	92.0 ± 111.6	132.8 ±139.6	58.03±62.27	76.5~353.4
Mn	13.79 ± 10.88	2.05 ± 2.29	1.61 ± 6.09	12.8 ± 1.70	2.54 ± 0.29	3.12 ± 4.16	8.11±18.46	2.39±6.18	/
Ni	4.65 ± 3.44	0.97 ± 1.53	0.63 ± 1.49	3.37 ± 0.55	0.87 ± 0.13	1.50 ± 1.50	7.97±8.62	0.39±0.33	/
Cu	5.57 ± 13.00	2.16 ± 3.00	1.33 ± 2.38	29.6 ± 3.74	0.98 ± 0.16	4.37 ± 2.12	/	/	1.0~4.0
Zn	27.03 ± 28.25	7.06 ± 7.88	4.46 ± 15.88	102.0 ± 30.1	14.7 ± 2.06	11.15 ± 6.93	52.24±51.89	25.41±29.96	/
Se	1.03 ± 0.91	0.24 ± 0.32	0.34 ± 0.73	0.68 ± 0.15	0.42 ± 0.05	/	0.81±0.69	0.22±0.39	/
Cd	42.62 ± 18.20	3.44 ± 1.63	7.92 ± 1.19	0.34 ± 0.05	0.11 ± 0.01	0.08 ± 0.06	/	/	0.1~0.6
Ba	20.50 ± 20.63	5.06 ± 4.60	2.81 ± 6.83	5.69 ± 0.78	0.57 ± 0.08	/	10.72±12.17	4.91±4.15	/
Pb	11.32 ± 6.49	1.85 ± 1.88	0.72 ± 1.56	25.3 ± 4.60	4.82 ± 0.66	2.74 ± 2.27	13.77±16.10	2.50±3.50	1.9~13.1
V	7.20 ± 6.62	0.55 ± 1.20	1.56 ± 3.44	1.43 ± 0.22	1.18 ± 0.10	0.81 ± 0.77	21.35±24.03	0.38±0.79	/
As	3.12 ± 8.96	0.39 ± 0.92	0.33 ± 1.13	1.35 ± 0.23	0.60 ± 0.07	0.51 ± 0.47	1.50±3.63	0.62±1.50	/

*Values with underlines indicate abnormally high concentrations, which were excluded from discussion in this study;
[#]TSP refers to total suspended particles in the atmosphere.

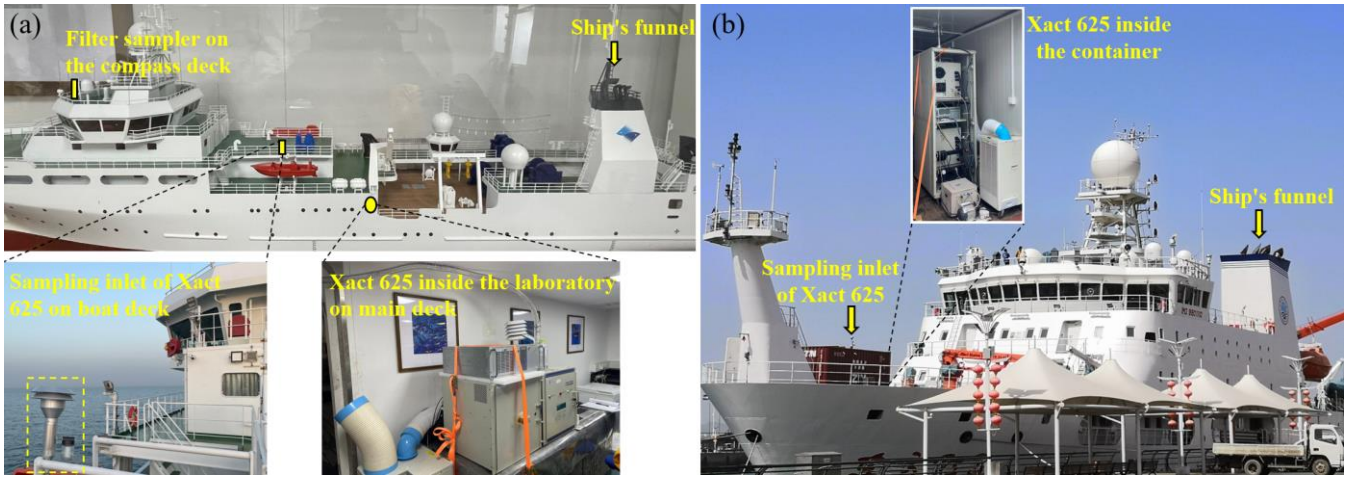

Figure S1. Instrument placement on research vessels. (a) BY cruise conducted aboard R/V *Lanhai 101*. (b) NWP1 and NWP2 cruises conducted aboard R/V *Dongfanghong 3*.

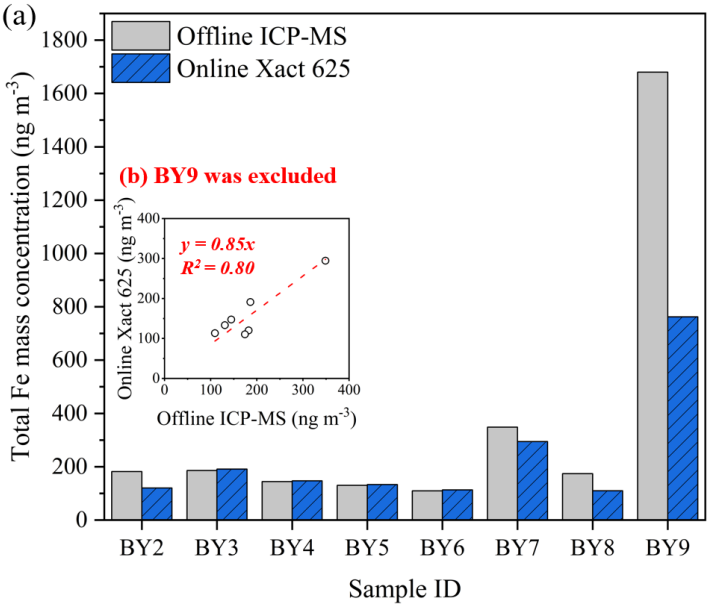

Figure S2. Comparison of atmospheric Fe concentrations measured by the online Xact 625 instrument and offline filter-based inductively coupled plasma mass spectrometry (ICP-MS) analysis during the BY cruise. (a) Bar charts comparing Fe concentrations measured by the two methods for samples collected during the BY2–BY9 sampling periods. (b) Scatter plot comparing Fe concentrations measured by the two methods for samples collected during the BY2–BY8 sampling periods. The BY1 filter sample is not shown because the online instrument data were incomplete during its sampling period.

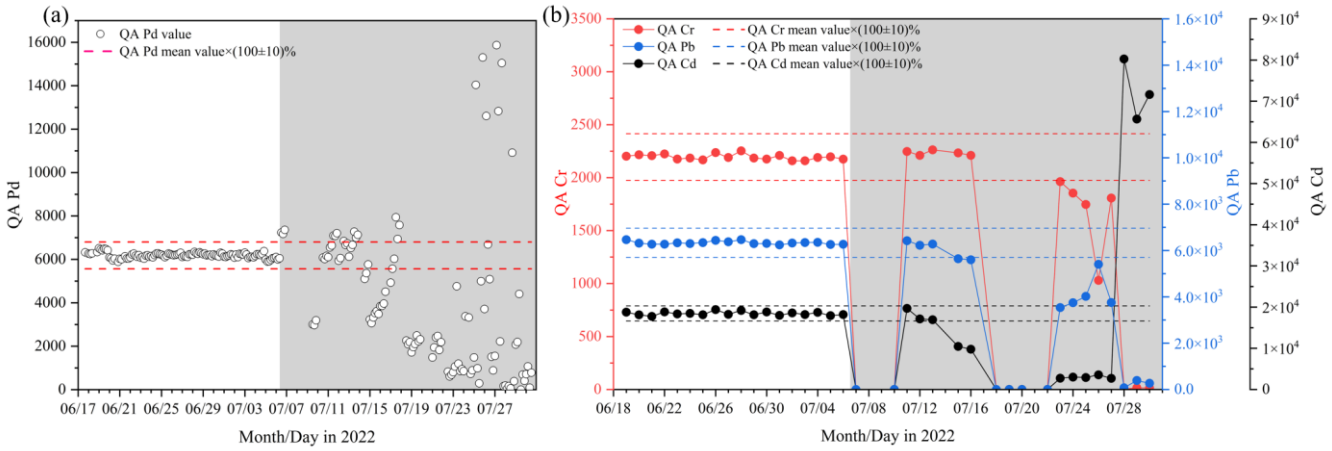

Figure S3. Automated quality control results from the Xact 625 instrument. (a) Automated analysis of the palladium rod. (b) Daily automated upscale rod check for Cr, Pb, and Cd. The two dashed lines represent ±10% deviation from the mean value, which was calculated based on measurements from June 18 to July 6, 2022.

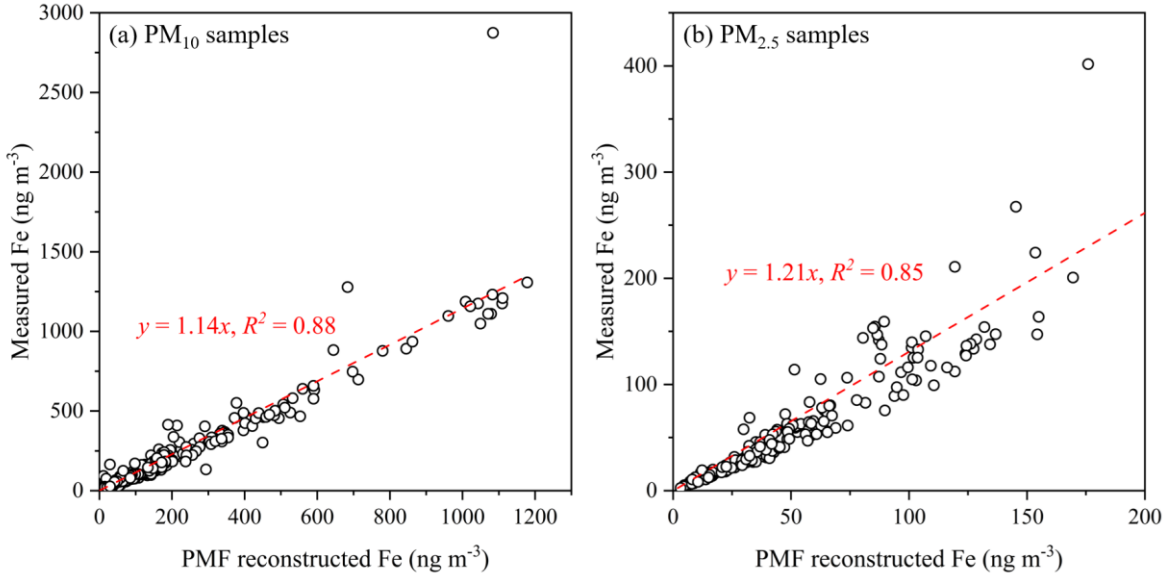

Figure S4. Scatter plots of the PMF reconstructed Fe concentrations and the measured Fe concentrations. The calculation method for PMF reconstructed Fe concentrations can be found in Equation (S4).

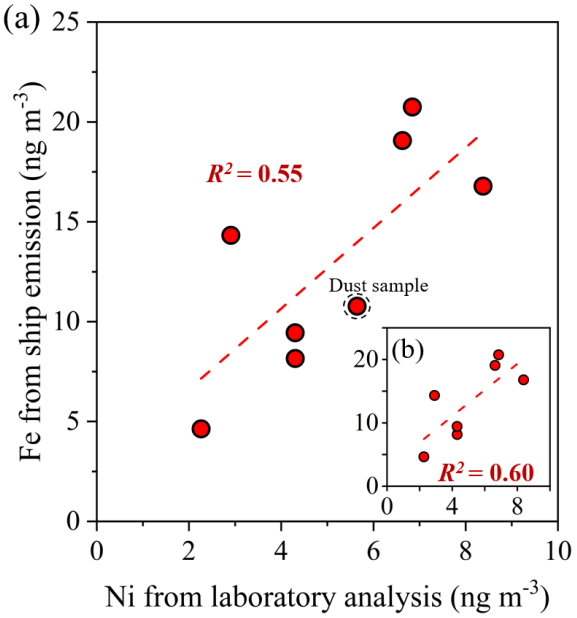

Figure S5. Comparison of ship-derived Fe concentrations resolved by PMF and online Xact 625 data versus Ni concentrations measured from offline filter analyses. (a) All samples; (b) excluding the dust-affected sample. The dashed circle indicates the dust sample, and the red dashed lines represent the linear regression lines.

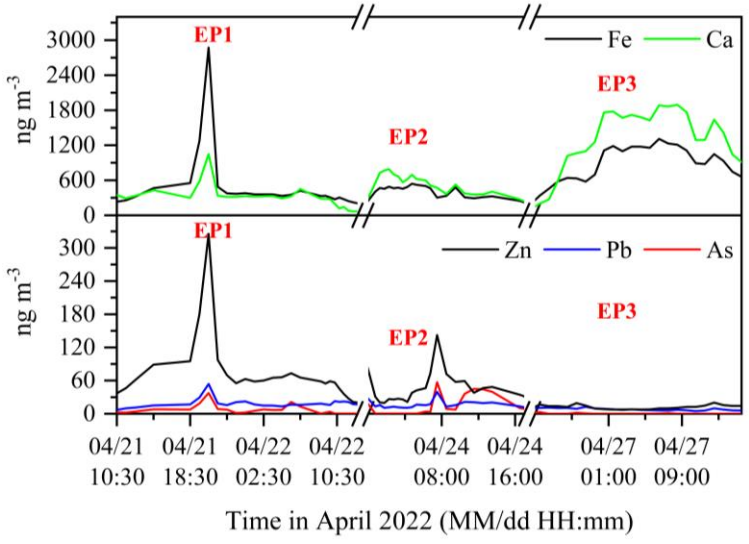

Figure S6. Concentration variations of different elements during the three high-Fe-concentration episodes during BY cruise. (a) Crustal elements (Ca and Fe) concentrations. (b) Pollution elements (Zn, Pb, and As) concentrations.

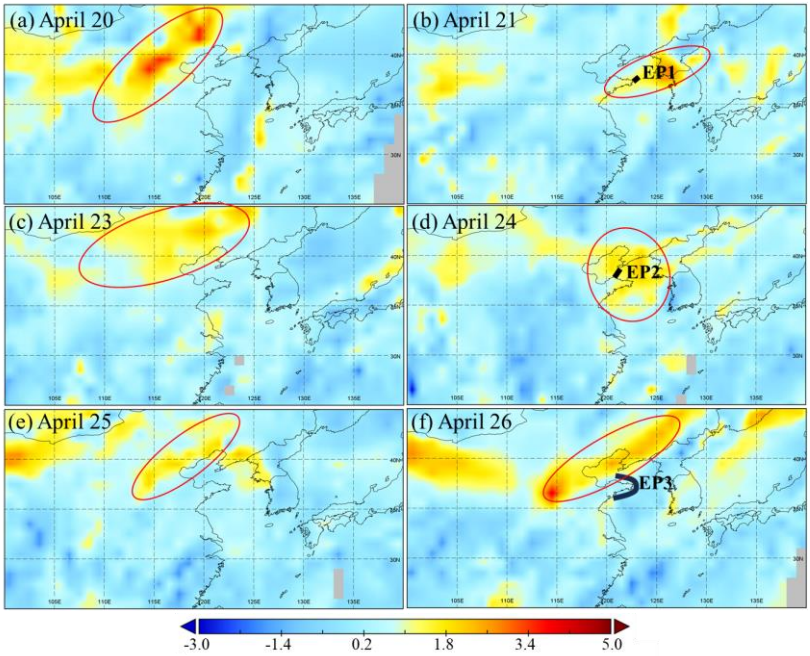

Figure S7. Spatial distributions of satellite-retrieved Absorbing Aerosol Index (AAI) during the three high-Fe-concentration episodes during BY cruise. Red ellipses highlight areas with high AAI values over upwind land regions or over the sea areas; black symbols mark sampling locations of EP1–EP3. Daily multi-sensor AAI products were provided by Tropospheric Emission Monitoring Internet Service (https://www.temis.nl/airpollution/absaai/, last access: 22 September 2025) .

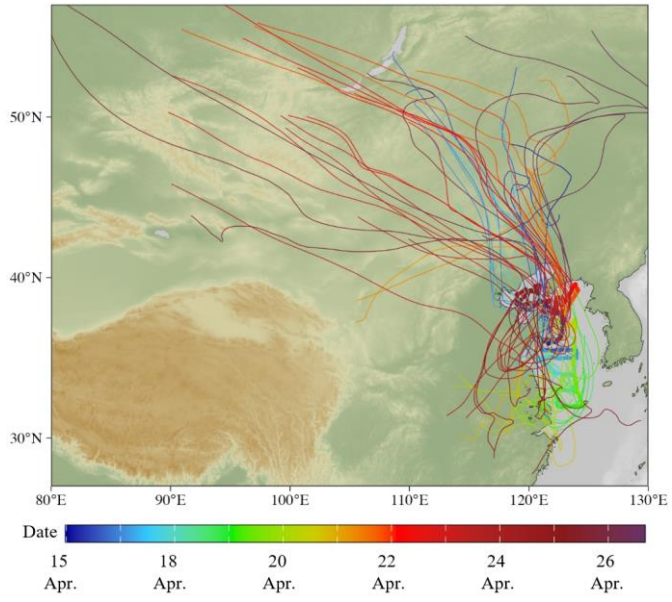

Figure S8. Seventy-two-hour backward air mass trajectories at 500 m altitude over the sampling regions during the BY cruise. The colours of the points and trajectories indicate the chronological sequence of the sampling times.

Figure S9. Photograph taken in the Yellow Sea on April 19, 2022. Vessels around the research vessel (*Lanhai 101*) are highlighted by red vertical boxes.

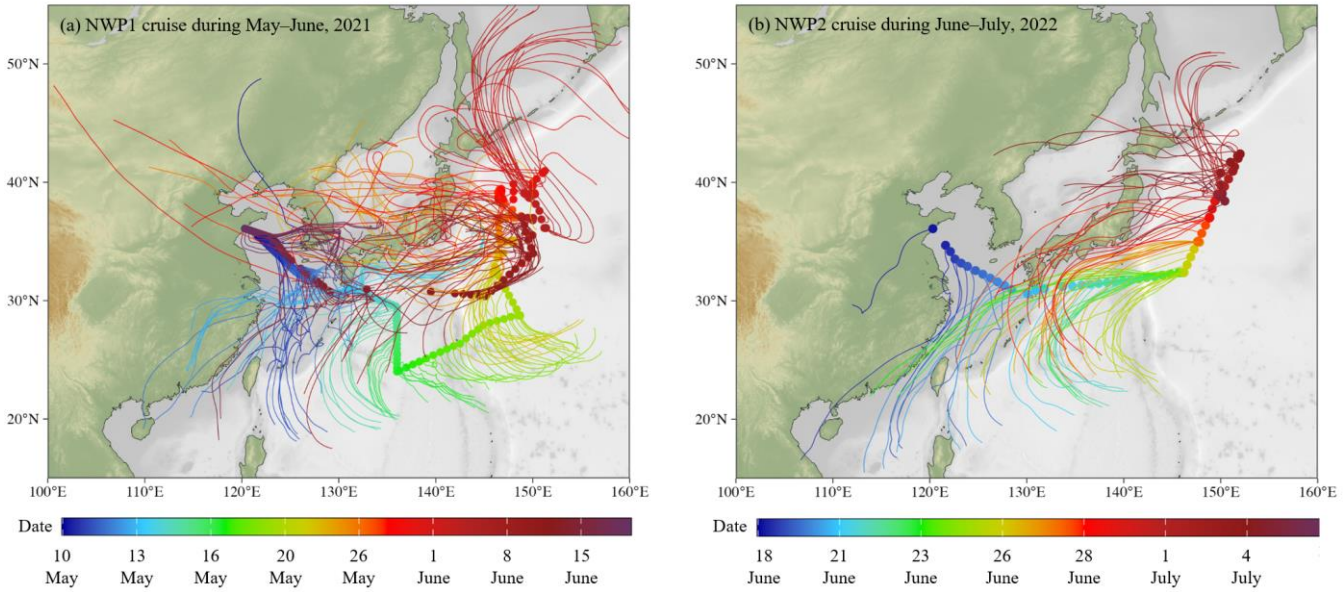

Figure S10. Seventy-two-hour backward air mass trajectories at 500 m altitude over the sampling regions during the NWP1 and NWP2 cruises. The colours of the points and trajectories indicate the chronological sequence of the sampling times.

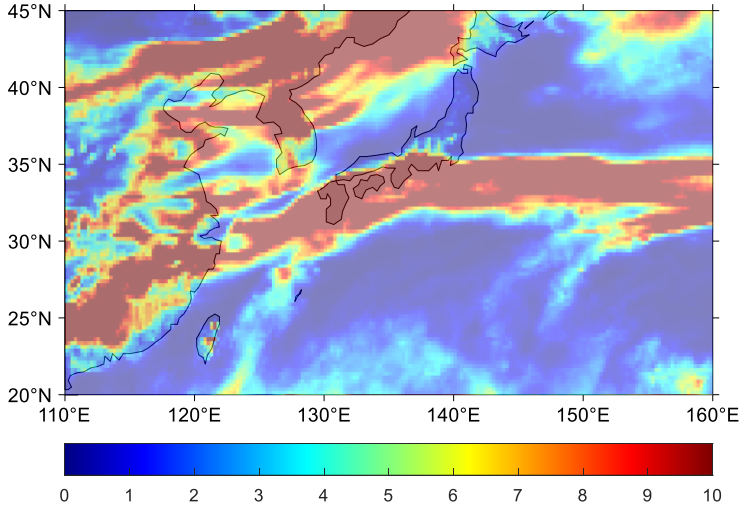

Figure S11. Mean precipitation (mm day^{-1}) over the Northwest Pacific from June 20 to 23, 2022. The NWP2 cruise track during this period was located south of the Japan and roughly overlapped with regions of enhanced precipitation. Data were from the European Centre for Medium-Range Weather Forecasts (ECMWF) Reanalysis v5 (ERA5) (Hersbach et al., 2023).

References

Gary, N., Rachelle, D., Steve, B., and Song, B.: EPA positive matrix factorization (PMF) 5.0 fundamentals and user guide, U.S. Environmental Protection Agency, Washington, USA, https://www.epa.gov/sites/default/files/2015-02/documents/pmf_5.0_user_guide.pdf (last access: 22 September 2025), 2014.

Ge, Y., Guan, W., Wong, K. H., and Zhang, R.: Spatial variability and source identification of trace elements in aerosols from Northwest Pacific Marginal Sea, Indian Ocean and South Pacific to Antarctica, Glob. Biogeochem. Cycle, 38, https://doi.org/10.1029/2024GB008235, 2024.

Hersbach, H., Bell, B., Berrisford, P., Biavati, G., Horányi, A., Muñoz Sabater, J., Nicolas, J., Peubey, C., Radu, R., Rozum, I., Schepers, D., Simmons, A., Soci, C., Dee, D., Thépaut, J-N.: ERA5 hourly data on single levels from 1940 to present. Copernicus Climate Change Service (C3S) Climate Data Store (CDS) [dataset], https://doi.org/10.24381/cds.adbb2d47, 2023.

Jin, T., Qi, J., Xi, Z., and Lin, X.: Impact of a dust event on the size distribution of metal elements in atmospheric aerosols at a coastal region and over the ocean, Environ. Sci., 40, 1562–1574, https://doi.org/10.13227/j.hjkx.201809012, 2019.

Shimada, K., Yang, X., Araki, Y., Yoshino, A., Takami, A., Chen, X., Meng, F., and Hatakeyama, S.: Concentrations of metallic elements in long-range-transported aerosols measured simultaneously at three coastal sites in China and Japan, J. Atmos. Chem., 75, 123–139, https://doi.org/10.1007/s10874-017-9366-8, 2018.

Zhang, H., Li, R., Dong, S., Wang, F., Zhu, Y., Meng, H., Huang, C., Ren, Y., Wang, X., Hu, X., Li, T., Peng, C., Zhang, G., Xue, L., Wang, X., and Tang, M.: Abundance and fractional solubility of aerosol iron during winter at a coastal city in Northern China: Similarities and contrasts between fine and coarse particles, J. Geophys. Res.-Atmos., 127, https://doi.org/10.1029/2021JD036070, 2022.

Zhang, T., Liu, J., Xiang, Y., Liu, X., Zhang, J., Zhang, L., Ying, Q., Wang, Y., Wang, Y., Chen, S., Chai, F., and Zheng, M.: Quantifying anthropogenic emission of iron in marine aerosol in the Northwest Pacific with shipborne online measurements, Sci. Total Environ., 912, https://doi.org/10.1016/j.scitotenv.2023.169158, 2024.